Defect Pattern of Highly Chiral Nematic Liquid Crystal Droplet

H. Y. Hui*
Department of Physics, The Chinese University of Hong Kong, Shatin, Hong Kong
(Dated: December 3, 2008)

Following previous researches on slightly chiral liquid crystals, we investigated on the corresponding configurations of highly chiral droplet. While in the case of lower chirality, a general structure can be predicted and experimentally verified, we find a semi-chaotic defect pattern is generated, as we slowly "tuned on" the chirality from slow to high. This paper summarizes the simulation procedures and phenomena observed with no theoretical background.

I. INTRODUCTION

Chiral liquid crystals droplets are of research interest because of its appearance in biological materials such as RNAs, and in display materials. Locally, when the scale becomes shorter than the natural pitch of the material, it has a is nematic-like structure. However on a large scale, the droplet demonstrates certain topological aspects that are of interests. First the defect pattern which is topological and is characteristic of the global structure; second, the topology (spherical) of the system at question which forces (by Poincaré constraint [1]) total surface topological charge of +2. With the assumption of complete surface-anchoring throughout the crystal, Bezić and Žumer [2] have theorized and summarized the equilibrium structures for various chirality. Experimental evidence using ZLI-4788-000–S-811 mixture [3], on the other hand, shows discrepancies with their predictions, and a successful theory is yet to be found.

In this paper, we follow another approach to the problem - that of numerical simulation. In sec. II I shall give the model used. In sec. III simulation results are summarized, with brief description of various indicators that were used. In sec. IV I shall address issues of subordinate importance.

II. MODEL

We use the Lebwohl-Lasher model [4] with lattice sites that form a jagged sphere. i.e., with a nearest-neighbor energy

$$\mathscr{V}_{ij} = -J\left(\mathbf{u_i}\cdot\mathbf{u_j}\right)^2 - K\left[\left(\mathbf{u_i}\times\mathbf{u_j}\right)\cdot\mathbf{r}_{ij}\right]\left(\mathbf{u_i}\cdot\mathbf{u_j}\right) \qquad (1)$$

where $\mathbf{u}_i$ is the director direction and $\mathbf{r}_{ij}$ is the vector pointing from site i to site j, and $J, K > 0$. A site is considered to be in the system if $\sqrt{x^2+y^2+z^2} < R$. To ensure surface anchoring, we add a layer of radial ghost spins [5] outside the sphere. The form of interaction between system spins and ghost spins has $J < 0$ and $K = 0$. This Hamiltonian favors twists between neighboring rotors and tangential rotors on surface.

To equilibriate the system, we first performed Monte Carlo (MC) simulations on zero chirality systems ($K = 0$), following Metropolis algorithm [6] with displacement parameters tuned to produce acceptance ratio about 50%. Chirality K was slowly increased to make sure equlibrium is kept as good as possible.

III. RESULTS

We looked from a number of perspectives to compare our results to previous theoretical and experimental findings. Bezić and Žumer [2], with the assumption of perfect tangential anchoring, predicts diametrical Frank-Pryce structure at high chirality and bipolar structure [7] at low chirality (different for different radii). For Frank-Pryce structure, the rotor orientations are

$$\hat{n}_d(r,\theta,\phi) = \cos\Omega\hat{\theta} + \sin\Omega\hat{\phi} \qquad (2)$$

with

$$\Omega = (s_0 - 1)\phi + qr$$

where (r,θ,ϕ) are the spherical coordinates with respect to the centre of the sphere, $q \propto K$ is inversely proportional to the natural pitch, and $s_0 = 1$ in the present case.

For bipolar structure, the rotor orientations are [8]

$$\hat{n}_b(r,\phi,z) = \sin\Lambda\hat{r} + \cos\Lambda\hat{z} \qquad (3)$$

with

$$\tan\Lambda = \frac{zr}{R^2 - z^2}$$

here (r,ϕ,z) are the cylindrical coordinates, and R the radius of sphere.

After minimization of free energy, Bezić and Žumer obtained the phase diagram as shown in Fig. 1.

In the following we present the results of numerical simulations.

A. Topological Defect Pattern

Half-integral topological defects are determined from the method of Zapotocky et al. [9], illustrated in Fig. 2. Implementation of this method on a lattice-site model means for every possible set of 4 neighbouring rotors forming a square, we traverse adjacent rotors one-by-one, and check if the direction has turned through 180° after returning to origin. If it

*Electronic address: to.hyin[at]gmail.com

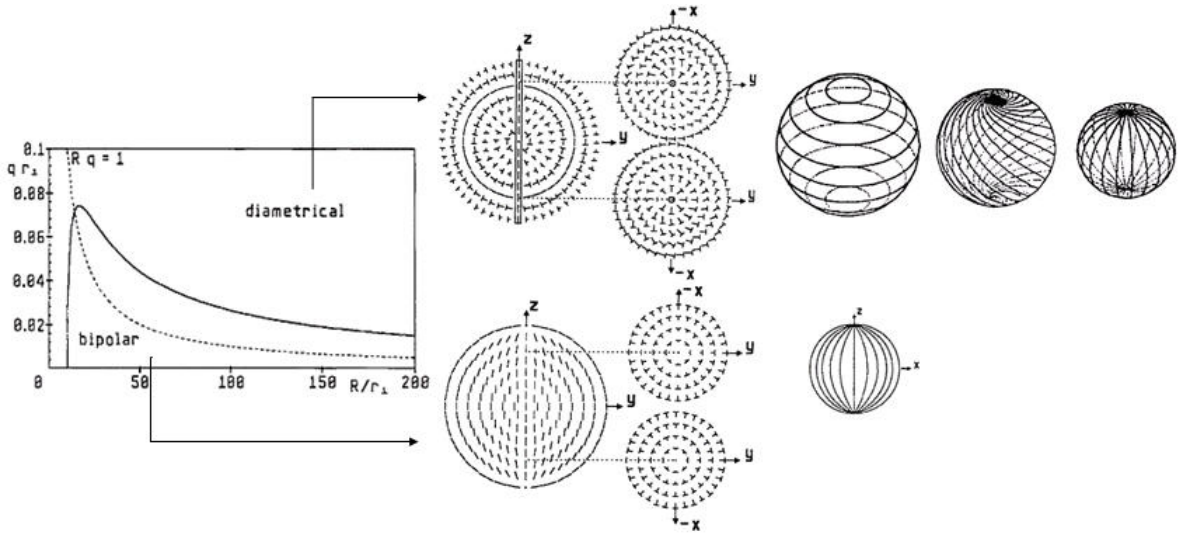

FIG. 1: The phase diagram predicted by Bezić and Žumer [2], as a function of chirality $K \propto q$ and radius R. Our simulation is at $R = 20$.

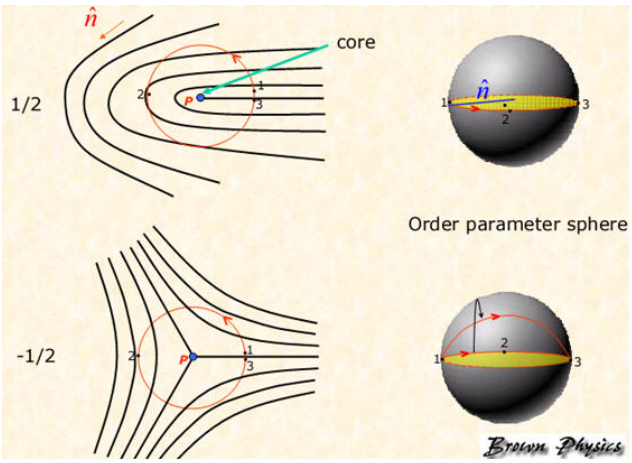

FIG. 2: The way to detect a point defect P is to go through a circle around it and trace out the change of the direction of the field (or molecules) along the loop in another paramter space. Upon completing a circle, if the order parameter go through only have a circle, there is a defect at P. (Image Courtesy Prof. Pelcovits)

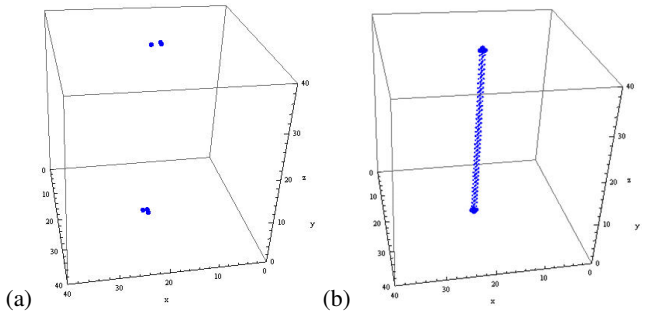

FIG. 3: The defect pattern for (a) bipolar structure and (b) diametrical structure. (b) is unstable, however, and it depicts the initial defect pattern for Eq. 2, with no MC applied.

does, this implies either a charge=$+\frac{1}{2}$ or $-\frac{1}{2}$ point defect at the centre of the square.

The shortcoming of this algorithm is that it can only detect a charge=$+1$ defect as two very near $-\frac{1}{2}$ defects. It also provides no clues for the escaped defects, i.e. those that have been eliminated through escape to 3rd dimension. This makes the defect pattern of the diametrical structure and that of bipolar structure similar, and other indicators, like the bipolar order parameter in sub-sec. III D, must be used to distinguish them.

Fig. 3 shows the pattern for bipolar and diametrical structures. It should be noted, however, that Fig. 3b is the "ideal" diametrical structure with no escape. After several MC steps are run on it, the pattern becomes similar to Fig. 3a. In our simulations, we find that for $K \lesssim 1$ in Eq. 1, the pattern is that of Fig. 3a, i.e. agrees with the theory of Bezić and Žumer. At values near $K = 1$, "chaotic" pattern slowly develops, as in Fig. 4. Two points to be noted: first, this critical value of K was hard to obtain, and a range about $0.95 < K < 1.1$ was found in different independent runs; second, the pattern appears to have inter-penetrating positively and negatively charged defect lines, which means it is not completely chaotic. It worths to be explored further.

B. Surface Defects

We define surface defects as topological defects that lies within 1 unit distance from the surface. They can be identified if properly visualized (Fig. 5). Due to Poincaré constraint, a continuous spherical model must have total surface defects +2. Because our current Lebwohl-Lasher model is discrete, inaccuracies are expected.

Note that for Frank-Pryce model, there is a topological defect at the $+z$ axis with charge s_0, and another at the $-z$ axis with charge $2 - s_0$.

One should refer back Fig. 3 and Fig. 4 and to verify

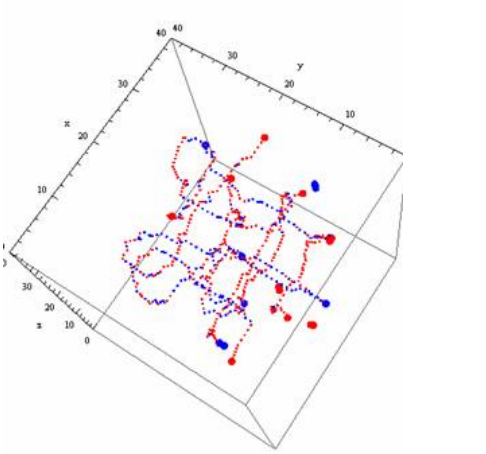

FIG. 4: Simulated defect patten for $K = 1.05$, in a particular run.

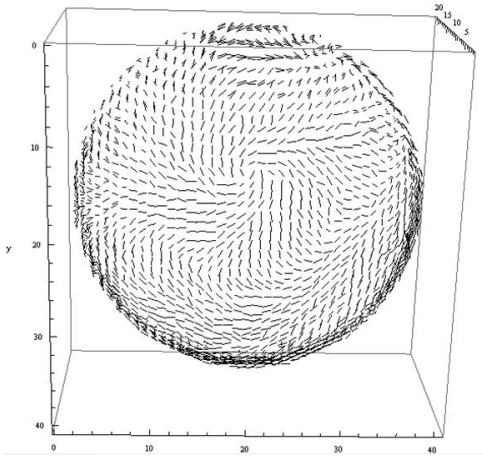

FIG. 5: An example of surface defect

Poincaré constraint. It is clear that for $K \lesssim 1$, there are charge $+1$ defects on the two natural poles of the droplet. For K large enough, however, one can find a number of "spurious" defects (unconnected to internal lines) sprung up and disappeared within several MC steps, usually occuring in pairs. This is because large chirality make those rotors near surface to twist a lot relative to each other, and since they are in contact with ghost spins, a large displacement could by chance occur and create them. For $K \gtrsim 1$, the "chaotic" pattern developed makes the track of surface defects difficult. It should be of interest to note that on average, one finds slightly more $-\frac{1}{2}$ defects than $+\frac{1}{2}$ defects, an apparent violation of Poincaré constraint. This could be possible because the model in use is discrete. However, a good explanation is unknown.

C. Optical Texture

Polarized optical textures are simulated using Müller matrix technique [7, 10]. It is used on lattice models to simulate the optical pattern that would be observed if two polarizers with cross polarization are put respectively at the top and the bottom of a droplet of liquid crystal, with light shown from the bottom. This is the main experimental technique by which experimenters probe the inner structure of a droplet of liquid crystal.

For the Müller matrix technique, first one initializes the Stokes vector to represent the polarization and intensity:

$$\mathbf{s} = \mathbf{s}_{\text{in}} = \begin{pmatrix} 1 \\ 0 \\ 0 \\ 0 \end{pmatrix}$$

The effect of passing through a polarizer corresponds multiplication of $\mathbf{s}$ by $\mathbf{P}$, which for a pair of cross-polarizer takes the form

$$\mathbf{P}_{0,90} = \frac{1}{2} \begin{pmatrix} 1 & 0 & 0 & \pm 1 \\ 0 & 0 & 0 & 0 \\ 0 & 0 & 0 & 0 \\ \pm 1 & 0 & 0 & 1 \end{pmatrix}$$

Then for each lattice site that the light passes, $\mathbf{s}_{in}$ is multiplied by

$$\mathbf{M}_j = \begin{pmatrix} 1 & 0 & 0 & 0 \\ 0 & \sin^2 2\phi_j + \cos^2 2\phi_j \cos\delta_j & -\cos 2\phi_j \sin\delta_j & \sin 2\phi_j \cos 2\phi_j (1-\cos\delta_j) \\ 0 & \cos 2\phi_j \sin\delta_j & \cos\delta_j & -\sin 2\phi_j \sin\delta_j \\ 0 & \sin 2\phi_j \cos 2\phi_j (1-\cos\delta_j) & \sin 2\phi_j \sin\delta_j & \cos^2 2\phi_j + \sin^2 2\phi_j \cos\delta_j \end{pmatrix}$$

In summary, the output Stokes vector is

$$\mathbf{s}_{\text{out}} = \mathbf{P}_{90} \Pi_j \mathbf{M}_j \mathbf{P}_0 \mathbf{s}_{\text{in}}$$

and outcome intensity is proportional to the first element in $\mathbf{s}_{out}$.

Xu and Crooker [3] have detailed the experimental optical textures for various chiralities, with a theoretical model that explains them well (Fig. 6). Our corresponding simulation result is given in Fig. 7. They display certain similar features but are quite different on the whole. A plausible explanation is the finite temperature used in MC simulation.

(a) 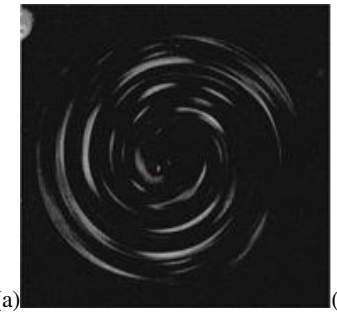 (b) 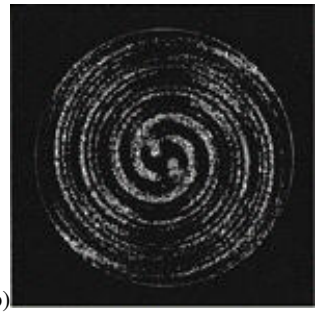

FIG. 6: (a) Optical texture of ZLI-4788-000–S-811 mixture with high chirality (Pitch<Radius) (b) Optical texture of a theoretical model developed by Xu and Crooker [3].

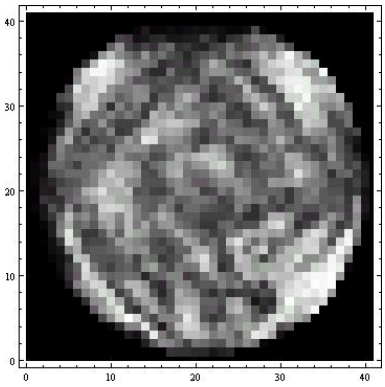

FIG. 7: Simulated optical texture using $K = 0.99$, with radius $R = 20$

D. Order Parameters

A number of order parameters are of interest. First, the radial parameters which tells how good the all-tangential assumption in Bezić and Žumer [2] holds:

$$R = \langle \hat{n} \cdot \hat{r} \rangle$$

Second, the bipolar order that can tell if the structure is close to a bipolar structure:

$$B = \langle \hat{n} \cdot \hat{n}_b \rangle$$

where $\hat{n}_b$ was given in Eq. 3.

Finally, the usual nematic order parameters used to quantify how uniformly aligned are the rotors:

$$S = \left\langle \frac{3}{2}\hat{n}_z^2 - \frac{1}{2} \right\rangle = \left\langle \frac{3}{2}\cos^2\theta_z - \frac{1}{2} \right\rangle$$

IV. ADDITIONAL

A. Molecular Dynamics

Another approach to numerial simulation is to use molecular dynamics with Gay-Berne overlap potential [11]. To account for the extended shape of liquid crystal molecules, it generalizes the usual 12-6 (Lennard-Jones) potential to:

$$U(\hat{u}_i, \hat{u}_j, \mathbf{r}) = 4\varepsilon(\hat{u}_i, \hat{u}_j, \hat{r}) \left[\left(\frac{\sigma_0}{r - \sigma(\hat{u}_i, \hat{u}_j, \hat{r}) + \sigma_0} \right)^{12} - \left(\frac{\sigma_0}{r - \sigma(\hat{u}_i, \hat{u}_j, \hat{r}) + \sigma_0} \right)^{6} \right]$$

where $\mathbf{r}$ is the intermolecular distance ($\hat{r}$ its unit vector) and $\hat{u}_i$ is the direction of each molecule. The necessary definitions are:

$$\sigma(\hat{u}_i, \hat{u}_j, \hat{r}_{ij}) = \sigma_0 \left[1 - \frac{\chi}{2} \left\{ \frac{[\hat{r} \cdot (\hat{u}_i + \hat{u}_j)]^2}{1 + \chi \hat{u}_i \cdot \hat{u}_j} + \frac{[\hat{r} \cdot (\hat{u}_i - \hat{u}_j)]^2}{1 - \chi \hat{u}_i \cdot \hat{u}_j} \right\} \right]^{-1/2}$$

$$\begin{aligned}
\varepsilon(\hat{u}_i, \hat{u}_j, \hat{r}) &= \varepsilon_0 \varepsilon^{\nu}(\hat{u}_i, \hat{u}_j) g^{\mu}(\hat{u}_i, \hat{u}_j, \hat{r}) \\
\varepsilon^{\nu}(\hat{u}_i, \hat{u}_j) &= \left[1 - \chi^2 (\hat{u}_i \cdot \hat{u}_j)^2 \right]^{-1/2} \\
g(\hat{u}_i, \hat{u}_j, \hat{r}) &= 1 - \frac{\chi'}{2} \left\{ \frac{[\hat{r} \cdot (\hat{u}_i + \hat{u}_j)]^2}{1 + \chi' \hat{u}_i \cdot \hat{u}_j} + \frac{[\hat{r} \cdot (\hat{u}_i - \hat{u}_j)]^2}{1 + \chi' \hat{u}_i \cdot \hat{u}_j} \right\} \\
\chi &= \frac{(\sigma_e/\sigma_s)^2 - 1}{(\sigma_e/\sigma_s)^2 + 1} \\
\chi' &= \frac{1 - (\varepsilon_e/\varepsilon_s)^{1/\mu}}{1 + (\varepsilon_e/\varepsilon_s)^{1/\mu}}
\end{aligned}$$

$$\begin{aligned}
\sigma_e/\sigma_s &= 3 \\
\mu &= 2 \\
\nu &= 1 \\
\varepsilon_s/\varepsilon_e &= 5
\end{aligned}$$

For spherical molecules, $\sigma_e/\sigma_s = 0$ and it reduces to Lennard-Jones Potential. This Gay-Berne potential is illustrated in Fig. 8.

Detailed algorithm was given in Billeter and Pelcovits [12]. Either leap-frog or Verlet algorithm can be used. Because of its intensive computation, it is more feasible with the implementation of neighbor-lists [13]. Quaternions [14] should also be used (to represent rotors' directions) to avoid computation of trigonometric functions.

Gay-Berne potential has the advantage that its parameters can be altered to represent isotropic, nematic, semectic A, and smectic B phases. During the evolution one can look into the radial distribution function, nematic order, and hexatic order [15] (for semetic phases). This approach was, however, not pursued in my project because with Lebwohl-Lasher model, one can investigate with much larger systems, and in nematic phase, liquid crystals have orderly structure as in the LL model.

B. Visualization

Tecplot, Mathematica, or other visualization packages can be used. The code for Mathematica, which was used in this

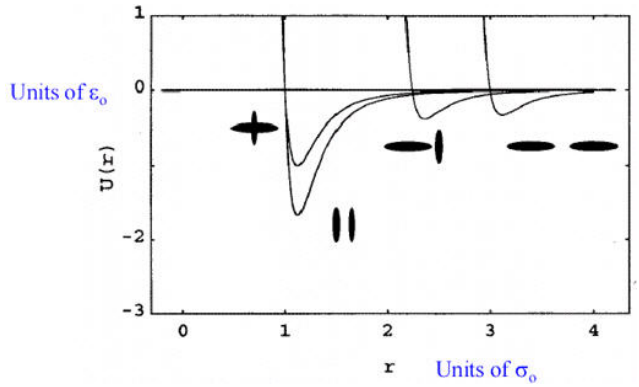

FIG. 8: The potential form for various relative orientations of the two molecules. The equilibrium distance is smallest for edge-to-edge orientation, and higher for end-to-end orientation. (Image Courtesy Prof. Pelcovits)

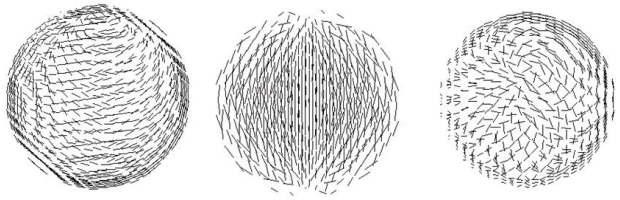

FIG. 9: The surface rotors for Frank-Pryce structures (left and right); All rotors in a bipolar structure (centre)

project, can be obtained from the author. A few examples are give in Fig. 9.

V. CONCLUSION

We have studied chiral nematic liquid crystal droplet solely using computer simulations. The results were compared and contrasted with previous theoretical and experimental results. We tried to extend the simulation to extremely high chirality and found a relatively complex structure would be formed.

Acknowledgments

The above work originated from the Summer Undergraduate Research Exchange program of the Chinese University of Hong Kong and Brown University. This research project in Brown University was supervised by Prof. Pelcovits. The author thanks him for his patience and help. The author expresses gratitude to both Physics Departments in Brown University and CUHK, for their cooperation and financial support.

[1] T. C. Lubensky and J. Prost, J. Phys. II **2**, 371 (1992).
[2] J. Bezić and S. Žumer, Liq. Cryst. **11**, 593 (1992).
[3] F. Xu and P. P. Crooker, Phys. Rev. E **56**, 6853 (1997).
[4] P. A. Lebwohl and G. Lasher, Phys. Rev. A **6**, 426 (1972).
[5] G. Skačej and C. Zannoni, Phys. Rev. Lett. **100**, 197802 (2008).
[6] N. Metropolis, A. W. Rosenbluth, M. N. Rosenbluth, A. H. Teller, and E. Teller, The Journal of Chemical Physics **21**, 1087 (1953).
[7] E. Berggren, C. Zannoni, C. Chiccoli, P. Pasini, and F. Semeria, Phys. Rev. E **50**, 2929 (1994).
[8] R. D. Williams, J. Phys. A: Math. Gen **19**, 1 (1986).
[9] M. Zapotocky, P. M. Goldbart, and N. Goldenfeld, Phys. Rev. E **51**, 1216 (1995).
[10] J. A. Schellman, *Polarization Spectroscopy of Ordered Systems* (Kluwer, Dordrecht, 1988).
[11] J. G. Gay and B. J. Berne, J. Chem. Phys. **74**, 3316 (1981).
[12] J. Billeter and R. Pelcovits, Comput. Phys. **12**, 440 (1998).
[13] M. P. Allen and D. J. Tildesley, *Computer Simulation of Liquids* (Oxford University Press, USA, 1989).
[14] A. Bulgac and M. Adamuţi-Trache, J. Chem. Phys. **105**, 1131 (1996).
[15] P. de Gennes and J. Prost, *The Physics of Liquid Crystals* (Oxford University Press, 1995).